European Conference on Computational Fluid Dynamics
ECCOMAS CFD 2006
P. Wesseling, E. Oñate and J. Périaux (Eds)

INFLUENCE OF NUMERICAL AND PHYSICAL PARAMETERS ON AN IMPLICIT PARTITIONED FLUID-STRUCTURE SOLVER

Marcus Heck*, Dörte C. Sternel, Michael Schäfer and Saim Yigit

Technical University of Darmstadt
Department of Numerical Methods in Mechanical Engineering,
Petersenstr. 30, D-64287 Darmstadt, Germany
*e-mail: heck@fnb.tu-darmstadt.de
web page: http://www.fnb.tu-darmstadt.de/

Key words: Fluid-Structure Interaction, Implicit Partitioned Solver, Sensitivity

Abstract. *The paper deals with an implicit partitioned solution approach for the numerical simulation of fluid-structure interaction problems. The method is realized on the basis of the finite-volume flow solver* FASTEST*, the finite-element structural solver* FEAP*, and the quasi-standard coupling interface MpCCI. Investigations concerning the influence of physical and numerical parameters on the efficiency and accurracy of FSI simulations involving laminar flows are discussed for a representative test case.*

1 INTRODUCTION

Coupled fluid-solid problems, which are characterized by the interaction of fluid forces and structural deformations occur in many applications in industry and science. For a realistic numerical simulation of such kind of problems one of the crucial issues is the algorithmic realization of the coupling mechanisms.

In the present paper we consider an implicit partitioned solution approach, which tries to combine the advantages of weakly and strongly coupled schemes in a complementary way. For each time step the (implicit) solution procedure consists in the application of different nested iteration processes for linearization, pressure-velocity coupling, and linear system solving, which are linked by a special predictor-corrector iteration for the fluid-structure coupling [5]. The method is realized on the basis of the finite-volume flow solver FASTEST [2], the finite-element structural solver FEAP [11], and the coupling interface MpCCI [7].

The considered approach gives a great deal of flexibility due to its modularity and the implicit predictor-corrector scheme ensures a strong numerical coupling which can be controlled by an underrelaxation.

The presented studies concern the influences of numerical parameters on the accuracy and efficiency of the coupled solver. In particular, the time step size and a structural

underrelaxation will be examined. Further, the influence of varying physical parameters of the fluid and the structure on the sensitivity of the coupled system and the efficiency of the coupled solver will be shown.

2 GOVERNING EQUATIONS

We consider a problem domain Ω consisting of a fluid part Ω_f and a solid part Ω_s, which regarding the shape as well as the location of fluid and solid parts can be arbitrary.

For the fluid domain part Ω_f we assume a flow of an incompressible Newtonian fluid. In this case the basic conservation equations governing transport of mass and momentum for a fluid control volume V_f with surface S_f are given by:

$$\frac{\mathrm{d}}{\mathrm{d}t}\int\limits_{V_\mathrm{f}} \rho_\mathrm{f}\,\mathrm{d}V_\mathrm{f} + \int\limits_{S_\mathrm{f}} \rho_\mathrm{f}(v_j - v_j^\mathrm{g})n_j\,\mathrm{d}S_\mathrm{f} \;=\; 0\,, \tag{1}$$

$$\frac{\mathrm{d}}{\mathrm{d}t}\int\limits_{V_\mathrm{f}} \rho_\mathrm{f} v_i\,\mathrm{d}V_\mathrm{f} + \int\limits_{S_\mathrm{f}} \left[\rho_\mathrm{f} v_j(v_i - v_i^\mathrm{g})n_j - T_{ij}\right]\,\mathrm{d}S_\mathrm{f} \;=\; \int\limits_{V_\mathrm{f}} \rho_\mathrm{f} f_{\mathrm{f}i}\,\mathrm{d}V_\mathrm{f}\,, \tag{2}$$

where v_i is the velocity vector with respect to Cartesian coordinates x_i, t is the time, ρ_f is the fluid density, and $f_{\mathrm{f}i}$ are external body forces (e.g., buoyancy forces). v_i^g is the velocity with which S_f may move (grid velocity) due to displacements of solid parts. The stress tensor T_{ij} for incompressible Newtonian fluids is defined by

$$T_{ij} = \mu_\mathrm{f}\left(\frac{\partial v_j}{\partial x_i} + \frac{\partial v_i}{\partial x_j}\right) - p\delta_{ij} \tag{3}$$

with the pressure p and the dynamic viscosity μ_f.

For the structure we assume a physically linear and geometrically nonlinear model. The basic balance equation for momentum for the solid domain Ω_s can be written as

$$\rho_\mathrm{s}\ddot{u}_i - \frac{\partial \sigma_{ij}}{\partial x_j} \;=\; \rho_\mathrm{s} f_{\mathrm{s}i}\,, \tag{4}$$

where u_i is the displacement, σ_{ij} denotes the Cauchy stress tensor, ρ_s is the density of the solid, and $f_{\mathrm{s}i}$ are external volume forces acting on the solid (e.g., gravitational forces). As constitutive relation the St. Venant-Kirchhoff material law is employed (e.g., [1]):

$$\boldsymbol{S} \;=\; \lambda_\mathrm{s}(\mathrm{tr}\boldsymbol{E})I + 2\mu_\mathrm{s}\boldsymbol{E} \tag{5}$$

with the second Piola-Kirchhoff stress tensor $\boldsymbol{S}$ and the Green strain tensor $\boldsymbol{E}$. λ_s and μ_s (shear modulus) are the Lamé constants which are related to the Youngs modulus E_s and the Poisson number ν_s by

$$\mu_\mathrm{s} = \frac{E_\mathrm{s}}{2(1+\nu_\mathrm{s})} \quad \text{and} \quad \lambda_\mathrm{s} = \frac{\nu_\mathrm{s}E_\mathrm{s}}{(1+\nu_\mathrm{s})(1-2\nu_\mathrm{s})}\,. \tag{6}$$

The problem formulation has to be closed by prescribing suitable boundary and interface conditions. On solid and fluid boundaries Γ_s and Γ_f standard conditions as for individual solid and fluid problems can be prescribed. For the velocities and the stresses on a fluid-solid interface Γ_i we have the conditions

$$v_i = \dot{u}_i^\mathrm{b} \quad \text{and} \quad \sigma_{ij} n_j = T_{ij} n_j \,, \tag{7}$$

where $\dot{u}_i^\mathrm{b}$ is the velocity of the interface.

3 NUMERICAL TECHNIQUES

For the discretization of the problem domain we follow a block-structuring technique. Domains with different fluid or solid parts are assigned to different blocks. Solid blocks are treated by the finite-element solver FEAP [11]. For the fluid blocks the parallel multigrid finite-volume flow solver FASTEST is employed [2, 8]. Both solvers involve second-order spatial discretizations and fully implicit second-order temporal discretizations, i.e., the BDF-2 method and the energy conserving Hilber-Hughes-Taylor method [4] for the fluid and structure equations, respectively.

For the fluid-structure coupling an implicit partitioned approach is employed [9]. In Figure 1 a schematic view of the iteration process, which is performed for each time step, is given. After the initializations the flow field is determined in the actual flow geometry. From this the friction and pressure forces on the interacting walls are computed, which are passed to the structural solver as boundary conditions. The structural solver computes the deformations, with which then the fluid mesh is modified, before the flow solver is started again.

For the mesh deformation an algebraic approach is employed [10]. Within the fluid solver a discrete form of the space conservation law

$$\frac{\mathrm{d}}{\mathrm{d}t} \int\limits_{V_\mathrm{f}} \mathrm{d}V = \int\limits_{S_\mathrm{f}} v_j^\mathrm{g} n_j \, \mathrm{d}S \tag{8}$$

is taken into account in order to compute the additional convective fluxes in (1)-(2). This is done via the swept volumes δV_c of the control volume faces for which one has the relation (see [3]):

$$\sum_c \frac{\delta V_c^n}{\Delta t_n} = \frac{V_\mathrm{f}^n - V_\mathrm{f}^{n-1}}{\Delta t_n} = \sum_c (v_j^\mathrm{g} n_j S_\mathrm{f})_c^n \,, \tag{9}$$

where the summation index c runs over the faces of the control volume, the index n denotes the time level t_n and Δt_n is the time step size. By this way interface displacements enter the fluid problem part in a manner strictly ensuring mass conservation.

The fluid-structure interaction (FSI) iteration loop is repeated until a convergence criterion is reached, which is defined by the change of the mean displacements:

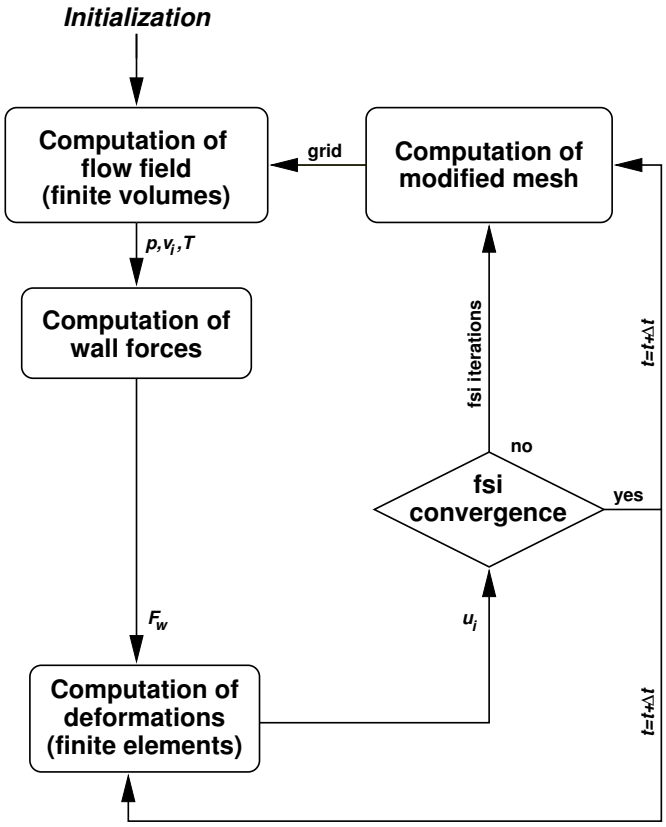

Figure 1: Flow chart of coupled implicit partitioned solution procedure

$$\Re^{\mathrm{FSI}} = \max_{i=1,2,3} \frac{\sum_{k=1}^{N} |u_i^{k,m-1} - u_i^{k,m}|}{N} < \varepsilon \,, \tag{10}$$

where m is the FSI iteration counter and N is the number of interface nodes.

The data transfer between the flow and solid solvers within the partitioned solution procedure is performed via an interface realized by the coupling library MpCCI [7]. In Figure 2 the corresponding information flow is represented schematically. MpCCI is used for controlling the data communication as well as for carrying out the interpolations of the data from the fluid and solid grids.

After the initialization MpCCI is provided with the geometry information at the fluid-solid interface for both grids. From the flow solver these are the coordinates of the control volume vertices and centers at the interface. From the structural solver only the node coordinates are required. With these geometry informations the forces at the nodes of the structural grid are interpolated and passed to the structural solver. The displacements from the structural solver at the nodes are transfered to MpCCI, which interpolates the displacements to the control volume vertices of the fluid grid interface. Afterwards the

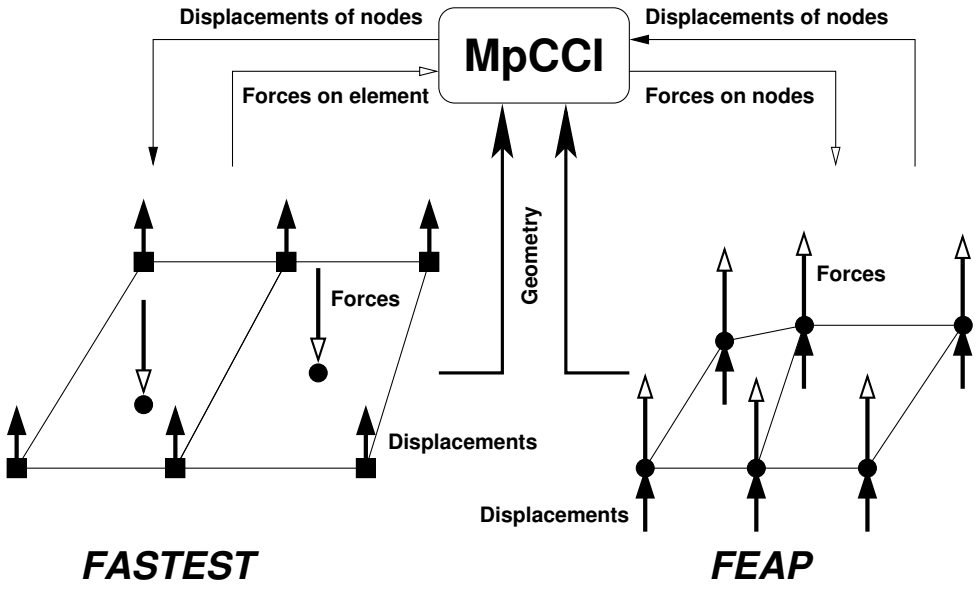

Figure 2: Schematic representation of information flow between fluid and solid solvers via the MpCCI interface

complete fluid grid is adapted and the corresponding coordinates of the control volume centers are computed. Finally, the new geometry informations are passed to MpCCI for the next iteration. An update of the geometry information of the solid grid is not necessary, since the structural finite-element computations always relate to the original solid grid. Note that there is no need for matching grids. For the necessary interpolations the conservative linear interpolation of MpCCI is employed [7].

To control the FSI iterations an underrelaxation approach is employed. Here the actually computed displacements u_i^{act} are (linearly) weighted with the values u_i^{old} from the preceding iteration to give the new displacements u_i^{new}:

$$u_i^{\text{new}} = \alpha_{\text{FSI}}\, u_i^{\text{act}} + (1 - \alpha_{\text{FSI}}) u_i^{\text{old}}\,, \tag{11}$$

where $0 < \alpha_{\text{FSI}} \leq 1$. Note that the underrelaxation does not change the final converged solution, but is employed because of its stabilizing effect. The basic effects of the underrelaxation has already been shown in [10]. In the present study we discuss its influence with respect to the efficiency of the numerical solution procedure and the grade of sensitivity of the FSI system.

In general, a sensitive system amplifies perturbations and can lead to fall-out or malfunction of the system. In a numerical FSI system the sensitivity can be characterized with the help of the structural displacements. A non-sensitive system does not overshoot and hence converges directly to the equilibrium. On the other hand, the system is sensitive, if the computated displacements tend to overpredict. If the overprediction is too strong this can lead to divergence of the computation. The sensitivity of an FSI system is directly related to the efficiency of the computation. If the structure displacements are

overpredicted the number of CFD iterations to obtain a converged solution is high. On the other hand if the structure does react more robust, the number of CFD iterations for a computation is low. Thus, the less sensitive the system the more efficient is the computation.

4 TEST CASE

As test case a three dimensional lid driven cubic cavity is considered (see Figure 3). The side length of the cube is $l = 1\,\mathrm{m}$. At the bottom a flexible membrane with thickness $t_{\mathrm{mem}} = 0.01\,\mathrm{m}$ is situated. The membrane is fixed at the edges and the lid moves with a time dependent lid velocity v_{lid} defined by

$$v_{\mathrm{lid}}(t) \quad = \quad \overline{v}_{\mathrm{in}} \left(1 - \cos\left(2\pi t / T_0\right)\right) \tag{12}$$

with the mean inflow velocity $\overline{v}_{\mathrm{in}}$ and the period $T_0 = 5\,\mathrm{s}$. The inlet and outlet have 10 % of the total height h_{in}=h_{out}=0.1 m and are situated in the upper part on the left and right sides, respectively. The inflow velocity corresponds to the lid velocity.

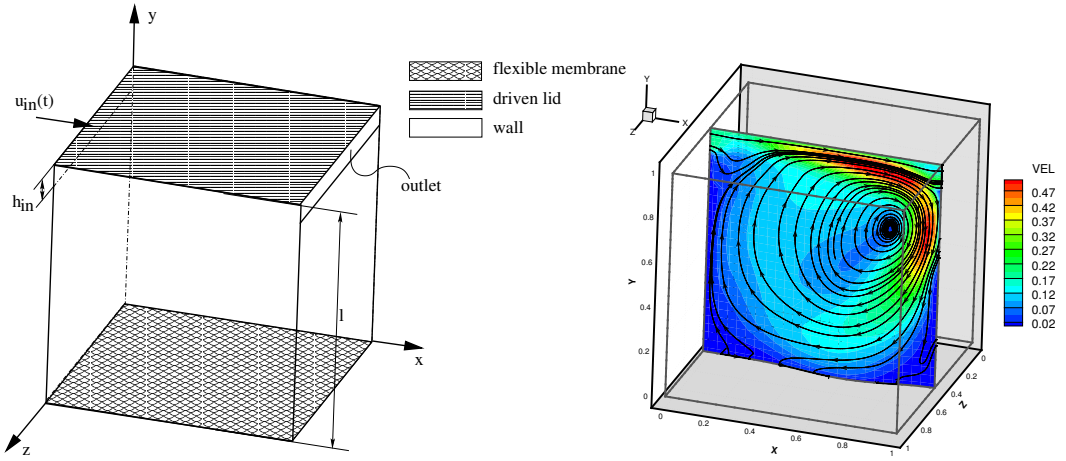

Figure 3: Test case configuration (left) and example velocity distribution with streamlines and deflected membrane (right).

For the investigation of the FSI system the following material parameters are varied:

- Youngs modulus $E_{\mathrm{s}} = 2500$, **5000**, $50000\,\mathrm{N/m^2}$,
- structure density $\rho_{\mathrm{s}} = 1000$, **500**, 1000, 2500, $5000\,\mathrm{kg/m^3}$,
- fluid density $\rho_{\mathrm{f}} = 2$, 5, **10**, $100\,\mathrm{kg/m^3}$,
- mean inflow velocity $\overline{v}_{\mathrm{in}} = 0.1$, 0.5, **1.0**, $2.0\,\mathrm{m/s}$.

The bold values indicate the default values if the corresponding parameter is not varied.

The number of iterations (which are directly proportional to the CPU time) are taken as measure for the efficiency of the FSI computation. In each case a simulation time of 0.5 s from a predefined flow field is computed.

5 NUMERICAL RESULTS

First the temporal discretization error is studied with help of the displacement vector in the middle of the membrane. Assuming that the finest time step provides the most accurate results this solution is taken as reference solution and the error is calculated relative to this. The mean error $\overline{e}$ finally represents the mean value of the error over the considered time interval and is defined as:

$$\overline{e} = \frac{\sum_{i=1}^{n} e_i}{n} \quad \text{with} \quad e_i = \left| 1 - \frac{u_i|_{\mathrm{MP}}}{u_{\mathrm{ref}i}|_{\mathrm{MP}}} \right| , \tag{13}$$

where n is the number of time steps and MP denotes the center point of the membrane with the coordinates $x = 0.5$, $y = 0.005$, and $z = 0.5$.

In Table 1 the errors resulting from computations with different time step sizes are indicated. As reference computation the time step size of $\Delta t = 0.001\,\mathrm{s}$ is taken. One can observe that the temporal error reacts less sensitive for small values of E_s, ρ_s, $\overline{v}_\mathrm{in}$ and large values of ρ_f. For all cases the error is within acceptable limits with respect to practical engineering applications.

In order to study the interaction of the time step size and the underrelaxation one fixed parameter set is computed with different time steps and different underrelaxation factors. In Figure 4 the number of required CFD iterations is plotted as against the underrelaxation factor α_FSI for the default test case. One can see that for every Δt an optimal α_FSI exists. The smaller Δt the smaller the optimal value of α_FSI. For small Δt the computation behaves more sensitive on changes of the underrelaxation factor than for large Δt. It appears that a large Δt makes a computation less sensitive. Small time steps even can lead to divergence of the computation as is the case for $\alpha_\mathrm{FSI} > 0.7$ and $\Delta t = 0.001\,\mathrm{s}$.

Next the influence of different physical parameters on the interaction of time step size and the underrelaxation is discussed. The results for an increased Youngs modulus E_s are shown in Figure 5. Again, the smaller Δt the more sensitive reacts the coupled system on changes in the underrelaxation. Decreasing the time step size one observes, that the optimal α_FSI for larger E_s tends to higher values. The computation also gets more sensitive, but at least it does not diverge. The number of required iterations at the optimal α_FSI for the default test case always is larger than for the more rigid structure with larger E_s. It also can be seen, that with the larger Youngs modulus the system behaves less sensitive with respect to changes in the underrelaxation.

Results for a lower fluid density $\rho_\mathrm{f} = 5\,\mathrm{kg/m^3}$ are shown in Figure 4. Comparing with the default case (see Figure 6) generally the same behavior can be seen. The large time

physical parameter		Error [%]		
E_s	2500	0.98	1.18	-
$[\mathrm{N/m^2}]$	5000	0.79	1.15	1.67
	50000	0.72	1.75	-
ρ_s	500	0.79	1.15	1.67
$[\mathrm{kg/m^3}]$	1000	0.44	0.64	-
	2500	0.85	1.98	-
	5000	1.21	2.85	-
ρ_f	2	1.34	2.86	3.99
$[\mathrm{kg/m^3}]$	5	0.74	1.82	-
	10	0.79	1.15	1.67
	100	-	2.07	2.24
$\overline{v}_\mathrm{in}$	0.1	0.80	2.16	4.62
$[\mathrm{m/s}]$	0.5	-	2.26	5.09
	1.0	0.79	1.15	1.67
	2.0	-	2.32	4.95
		0.002	0.005	0.01
		time step size Δt [s]		

Table 1: Temporal discretization error for different material parameters depending on the time step size.

step again represents the most efficient computation. Further decreasing the fluid density leads to a similar behavior of the coupled system as when increasing the Youngs modulus.

In the following examinations the underrelaxation factor is varied for different material parameters while keeping the time step size fixed.

In Figure 7 the number of CFD iterations is plotted as against the underrelaxation factor α_FSI for varying material parameters E_s. Looking for the optimal α_FSI one can see, that the bigger the Youngs modulus the more efficient is the computation. Also, the stiffer the structure the less sensitive is the coupled system on changes of α_FSI. Another observation is that the optimal α_FSI increases by increasing the Youngs modulus. For higher values of α_FSI than the optimal one the sensitivity increases and, therefore, the efficiency decreases. This even can lead to divergence of the coupled system, like with $E_\mathrm{s} = 2500\,\mathrm{kg/m^3}$ for $\alpha_\mathrm{FSI} > 0.6$, or $E_\mathrm{s} = 5000\,\mathrm{kg/m^3}$ for $\alpha_\mathrm{FSI} > 0.7$. Computations with values lower than the optimal α_FSI behave robust, but more iterations are required, i.e. again the efficiency decreases.

The results for varying fluid density ρ_f are shown in Figure 8. Here, the behavior is opposite. The larger the density the more sensitive is the behavior of the coupled system and the more one has to underrelax the computation. The optimal α_FSI decreases with increasing fluid density.

As a further aspect we study the influence of the physical parameters on the sensitivity. In Figures 9–12 the number of iterations is plotted as against the physical parameters E_s,

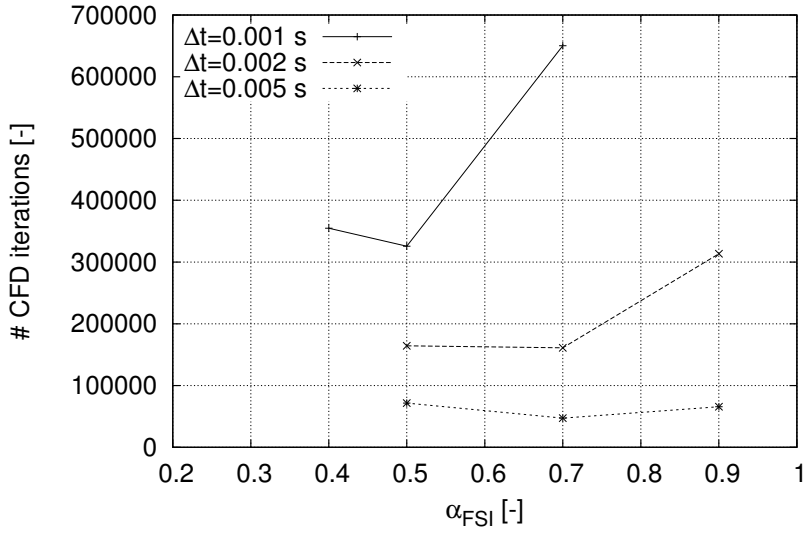

Figure 4: Influence of time step size and underrelaxation on the number of CFD iterations for default test case with $\rho_\mathrm{s} = 500\,\mathrm{kg/m^3}$, $E_\mathrm{s} = 5000\,\mathrm{N/m^2}$, $\rho_\mathrm{f} = 10\,\mathrm{kg/m^3}$, $\overline{v}_\mathrm{in} = 1\,\mathrm{m/s}$.

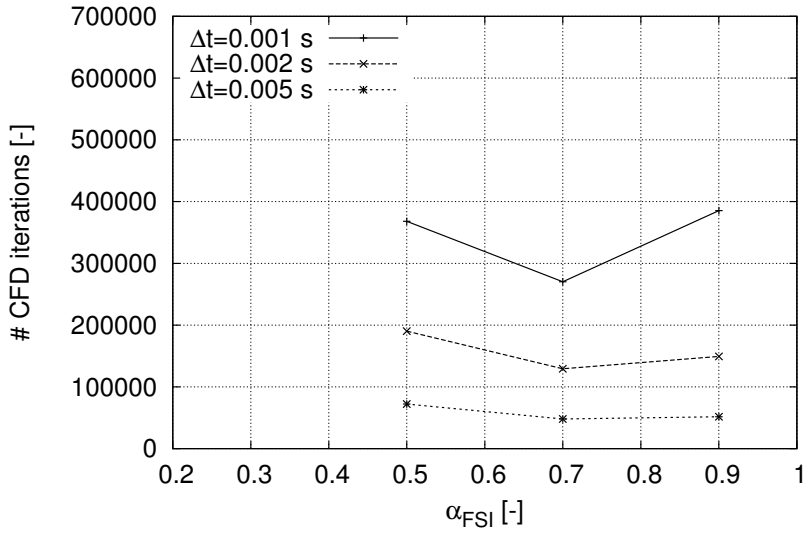

Figure 5: Influence of Δt and α_FSI on the number of CFD iterations with $E_\mathrm{s} = 50000\,\mathrm{N/m^2}$.

ρ_s, ρ_f, and $\overline{v}_\mathrm{in}$, respectively. In all cases results with $\alpha_\mathrm{FSI} = 0.7$ are shown.

Increasing the structural parameter E_s (see Figure 9) the computation gets more robust and, therefore, more efficient. This effect is the stronger the smaller the chosen Δt. For example with $\Delta t = 0.001\,\mathrm{s}$ increasing the Youngs modulus from $E_\mathrm{s} = 5000\,\mathrm{kg/m^3}$ to $E_\mathrm{s} = 50000\,\mathrm{kg/m^3}$ one needs less than the half of the number of iterations.

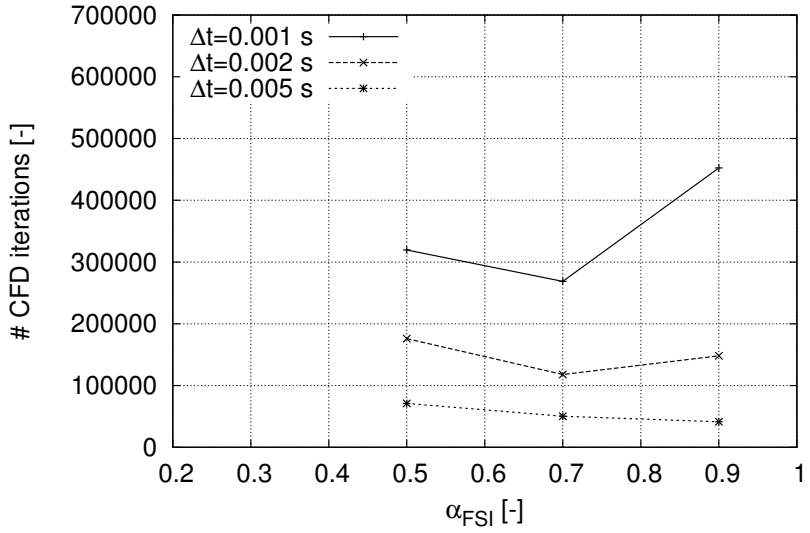

Figure 6: Influence of Δt and α_{FSI} on the number of CFD iterations with $\rho_{\mathrm{f}} = 5\,\mathrm{kg/m^3}$.

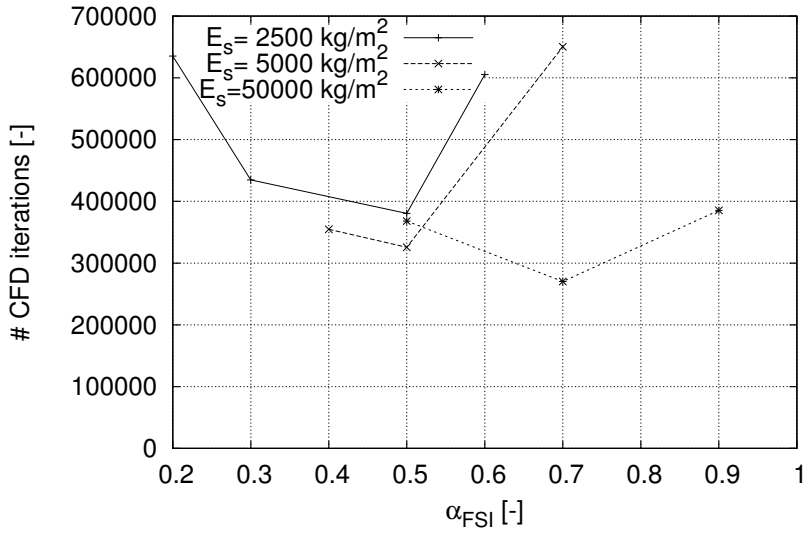

Figure 7: Influence of α_{FSI} on the number of CFD iterations with $\Delta t = 0.001\,\mathrm{s}$ for different E_{s}.

For increasing structural density (see Figure 10), like for the Youngs modulus, the computation needs less iterations, i.e. is less sensitive. This effect is most pronounced for the smallest $\Delta t = 0.001\,\mathrm{s}$ and seems to go to a limit, e.g. for $\Delta t = 0.001\,\mathrm{s}$ at about 200000 iterations.

For the fluid density the effect is opposite (see Figure 11). Increasing ρ_{f}, the computation gets more sensitive. This best can be seen for the smallest time step $\Delta t = 0.001\,\mathrm{s}$.

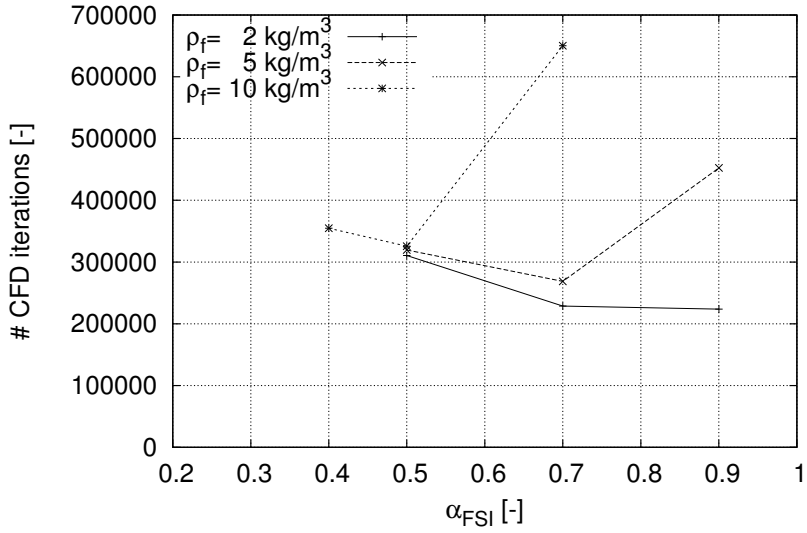

Figure 8: Influence of α_{FSI} on the number of CFD iterations with $\Delta t = 0.001\,\mathrm{s}$ for different ρ_{f}.

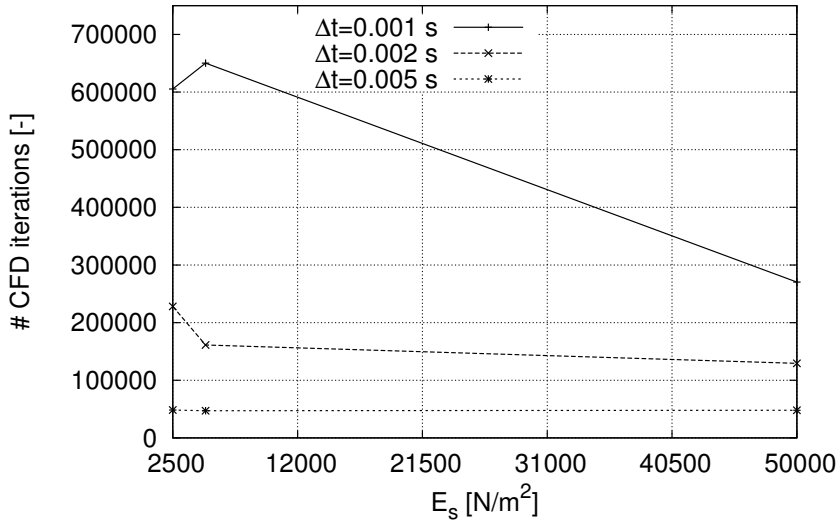

Figure 9: Effect on sensitivity of the FSI system for varying Youngs modulus E_{s} with different Δt and $\alpha_{\mathrm{FSI}} = 0.7$.

The inflow velocity (see Figure 12) does not have big effect on the sensitivity of the FSI system. For all values the computation is most efficient with bigger time steps.

In the partitioned fluid-structure solver employed the efficiency not only depends on the CFD iterations, because it also involves the structural solver and the coupling library. The

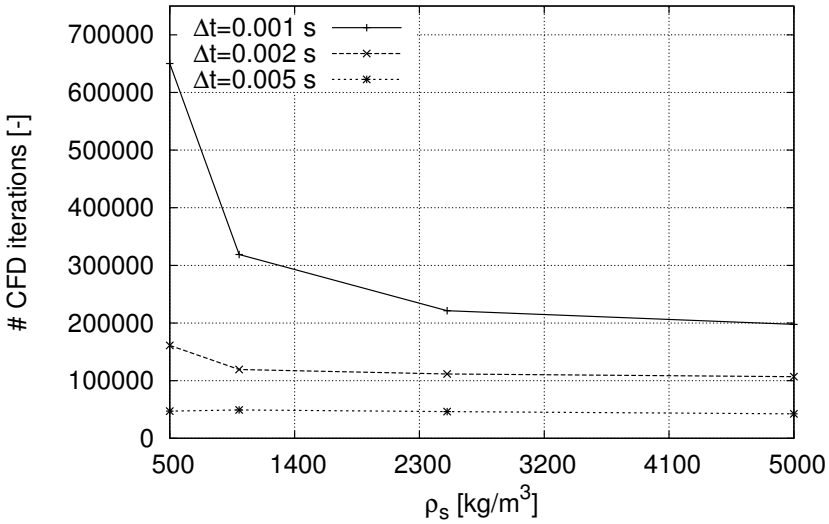

Figure 10: Effect on sensitivity of the FSI system for varying structure density ρ_{s} with different Δt and $\alpha_{\mathrm{FSI}} = 0.7$.

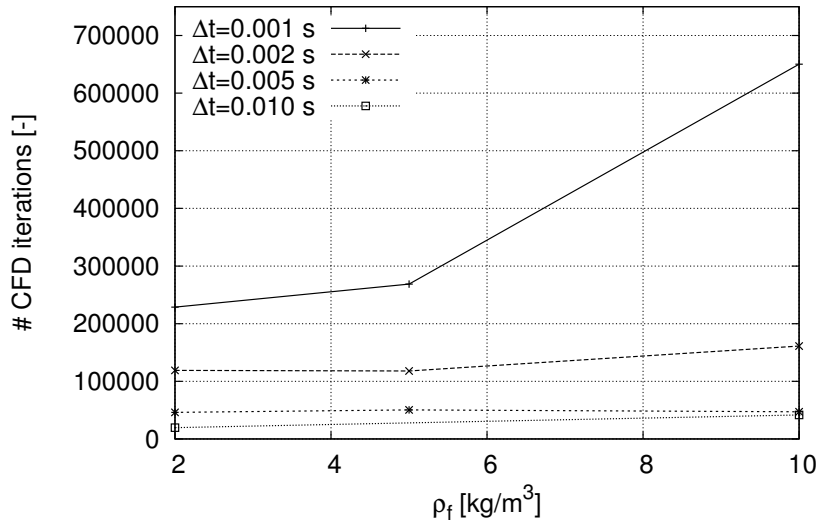

Figure 11: Effect on sensitivity of the FSI system for varying fluid density ρ_{f} with different Δt and $\alpha_{\mathrm{FSI}} = 0.7$.

time spent for the computations of the interpolations and the data transfer is negligible. In Figure 13 and 14 the mean number of coupling steps depending on the underrelaxation for the whole computation is plotted. One can see, that for a fixed structural underrelaxation the mean number of coupling iterations per time step does not depend much on the time

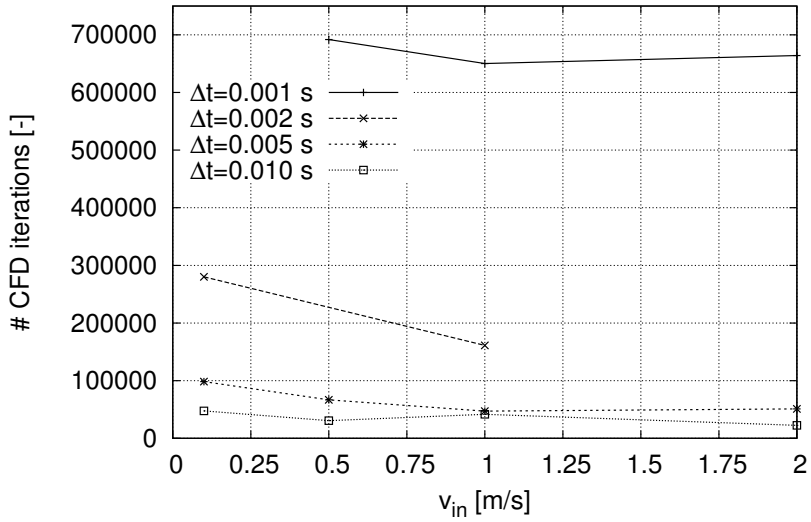

Figure 12: Effect on sensitivity of the FSI system varying inflow velocity $\overline{v}_{\text{in}}$ with different Δt and $\alpha_{\text{FSI}} = 0.7$.

step size.

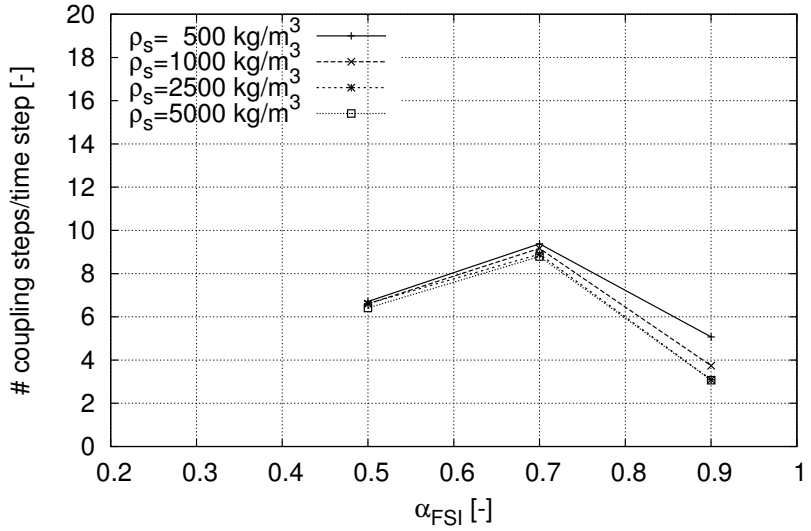

Figure 13: Comparison of required coupling steps for different α_{FSI} for varying structure density ρ_{s} with $\Delta t = 0.005\,\text{s}$.

All previous investigations concerned a computation of $t = 5\,\text{s}$ simulation time. Finally, the behavior during one time step is examined. Only one representative time step is considered. In Figure 15 the computation time for the structural and fluid solvers for the

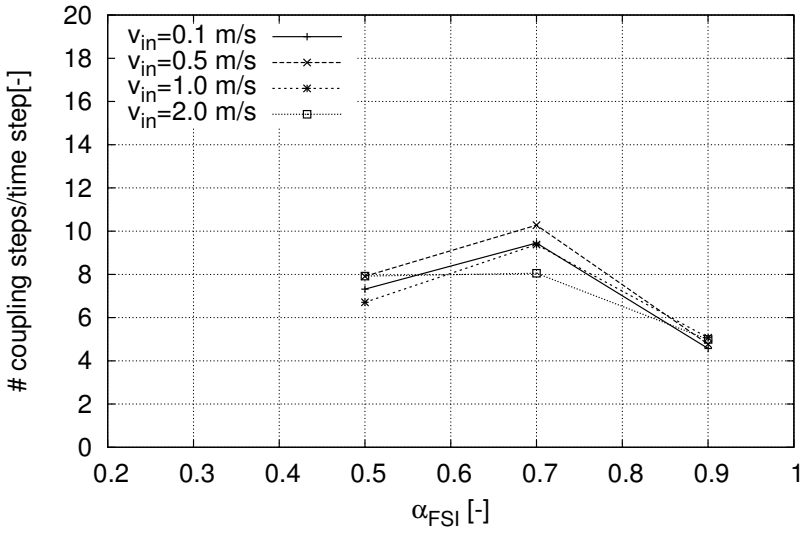

Figure 14: Comparison of required coupling steps for different α_{FSI} for varying inflow velocity $\overline{v}_{in}$ with $\Delta t = 0.005\,\text{s}$.

coupling steps are plotted. It can be seen, that the computational time required by the flow solvers decreases from FSI iteration to FSI iteration. The computational time for the flow problem decreases faster than the one for the structural problem, which only slightly speed up during the time step.

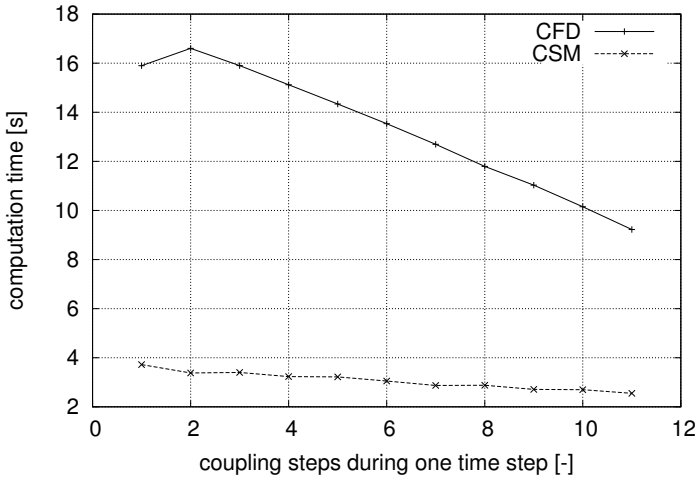

Figure 15: Computation time for consecutive coupling steps for fluid (CFD) and structure (CSM) subproblem for one representative time step.

6 CONCLUSIONS

An implicit partitioned approach for the numerical simulation of fluid-structure interaction has been studied with respect to its behavior when varying numerical and physical parameters. It has been shown, that large time steps have a stabilizing effect on the FSI system and make the computation less sensitive with respect to underrelaxation. It turned out that the number of coupling steps only weakly depends on the time step size. Of course, a larger time step size increases the temporal discretization error, but it was within acceptable limits for all considered cases.

Further it could be shown that increasing the Youngs modulus E_s or the structure density ρ_s or decreasing the fluid density ρ_f lowers the sensitivity of the FSI system. The less sensitive the system the faster it can be solved by the coupled implicit partitioned solver.

Acknowledgements

The financial support of the work by the Deutsche Forschungsgemeinschaft within the Research Unit 493 *Fluid-Structure Interaction: Modelling, Simulation, Optimization* is gratefully acknowledged.

REFERENCES

[1] D. Braess. *Finite Elements*, second edition, Cambridge University Press, 1996.

[2] FASTEST – *User Manual, Department of Numerical Methods in Mechanical Engineering*, Technische Universität Darmstadt, 2004.

[3] J. Ferziger, M. Perić, *Computational Methods for Fluid Dynamics*, Springer, Berlin, 1996.

[4] H.M. Hilber, T.J.R. Hughes, and R.L. Taylor. *Improved numerical dissipation for time integration algorithms in structural dynamics*. Earthquake Engineering and Structural Dynamics, 5:282-292, 1977.

[5] H. Lange. *Methoden zur numerischen Simulation des strömungs- und strukturmechanischen Verhaltens von Labyrinthdichtungen*, Dissertation, Department of Numerical Methods in Mechanical Engineering, Technische Universität Darmstadt, 2004.

[6] S. Meynen, J. Mayer, and M. Schäfer. *Coupling Algorithms for the Numerical Simulation of Fluid-Structure Interaction Problems*. In ECCOMAS 2000 Proceedings (CD-ROM), 15 pages, Barcelona, 2000.

[7] *MpCCI – Mesh-Based Parallel Code Coupling Interface. User Guide V2.0*, SCAI, 2004.

[8] M. Schäfer, S. Meynen, R. Sieber, and I. Teschauer. *Efficiency of Multigrid Methods for the Numerical Simulation of Coupled Fluid-Solid Problems*. In P. Minev and Y. Lin (eds.), Scientific Computing and Applications, Advances in Computation: Theory and Practice, pages 257–266, Nova Science Publishers, Huntington, 2001.

[9] M. Schäfer, H. Lange, and M. Heck. *Implicit Partitioned Fluid-Structure Interaction Coupling*. In Proceedings of 1er Colloque du GDR Interactions Fluide-Structure, pages 31–38, Sophia Antipolis (France), 2005.

[10] M. Schäfer, M. Heck and S. Yigit *An Implicit Partitioned Method for Numerical Simulation of Fluid-Structure Interaction*. In Lecture Notes in Computational Science and Engineering 53 (34595-7), Springer, Berlin, to appear 2006.

[11] R.L. Taylor. FEAP – *A Finite Element Analysis Program. Version 7.4 User Manual*. University of California at Berkeley, 2002.

[12] J.F. Thompson, B.K. Soni, and N.P. Weatherill. *Handbook of Grid Generation*. CRC Press LLC, 1999.